Thermal Features of Low Current Discharges and Energy Transfer to Insulation Surfaces

An Xiao, Simon M. Rowland
University of Manchester
School of Electrical of Electronic Engineering,
Oxford Road, Manchester, M13 9PL, United Kingdom

and **Xin Tu**
University of Liverpool
Department of Electrical Engineering and Electronics
Brownlow Hill, Liverpool, L69 3GJ, United Kingdom

and **J. Christopher Whitehead**
University of Manchester
School of Chemistry
Oxford Road, Manchester, M13 9PL, United Kingdom

ABSTRACT

The thermal features of low current AC discharges, of between 2 and 5 mA, between water droplets are presented in this paper. The 'Best-fit' method of optical emission spectroscopy (OES) analysis is applied to measure the discharge temperature. The discharge temperature increased from 1200 K to 1500 K when the current level rose from 2.5 mA to 5 mA, and its temperature was less sensitive to arc length than arc current. Measurements of the distribution of temperature along a 4 mm discharge showed that the regions including the arc roots do not have a higher temperature than the discharge column, despite appearing brighter. The introduction of a silicone rubber insulation surface adjacent to the discharge increased the discharge temperature, typically by ~160 K, and its energy per half cycle by 150%. The resulting temperature distribution on the insulation surface was captured by infrared thermal imaging. Finite element analysis (FEA) software successfully simulated heat transfer between discharge and surface, and showed good agreement with experimental results: highest temperatures being seen under the centre of the arc, where damage is also first seen in practice. FEA can thus be used to model, for example, the impact of thermal conductivity on insulation surface temperature.

Index Terms - **thermal**, **temperature**, **electrical discharge, arc, plasma diagnostics, FEA, optical emission spectroscopy, OES, insulation surface, heat transfer**

1 INTRODUCTION

CONVENTIONALLY, glass and ceramic insulators have been used to isolate high voltage overhead conductors from their supporting towers. In recent years composite insulators, using materials such as silicone rubber, have been installed on power systems because of their features of low weight, high mechanical strength and competitive cost [1]. In contrast with ceramics, insulators featuring polymeric surfaces may be degraded by solar UV radiation, organic contamination and the presence of electrical discharges. As such insulators are key components for the security and safety of the system [2], their ageing processes are of great importance. Modern polymeric insulators generally perform well and reliably, which means that understanding of the longer-term processes of ageing has become more important, being required for longer term asset management strategies. Here the long-term effects of low current level discharges on wet insulation surfaces are considered.

Generally speaking, discharges over insulation surfaces can be divided into two kinds: The first kind are high current discharges greater than 10 mA, which are associated with dry-band formation and may, if the current increases, lead to flashover events. These have been studied widely [3, 4]. The second kind is low current discharges of less than 10 mA such as corona and inter-droplet arcs, which have been less widely considered in this context. The high current discharge has relatively high energy levels but their probability of occurrence

Manuscript received on 30 January 2014, in final form 23 April 2014, accepted 23 April 2014.

DOI 10.1109/TDEI.2014.004587

is low, while the low current discharges with less power may be quite common and may be present over the insulator surface for thousands of hours in its lifetime [5–7]. The preceding comments are not quantified, and it is not known which type of discharge dominates the ageing of the surface of a real insulator. The work reported here considers a heat transfer model between a low-current discharge and an insulation surface, which allows an informed discussion over the likelihood of long-term low-current discharge activity damaging a polymer surface. The aim is to create a model capable of predicting the ageing of an insulation surface in the presence of such discharges. To build such a model it is necessary first to know the temperature of the discharge column.

In the work reported here the 'Best Fit' spectroscopy method is used to experimentally determine the temperature of discharge plasmas [8–10]. The temperatures of AC discharges under various conditions have been measured and analysed. These experimental results have then been used in finite element analysis to build an energy transfer model between the discharge and material surface.

2 BACKGROUND

2.1 PRINCIPLE OF THE 'BEST-FIT' METHOD

A plasma is a state of matter similar to a gas in which a portion of the particles are ionized. It is an electrically neutral mixture of electrons, positive and negative ions, and neutral particles [11, 12]. Based on their thermal characteristics, two types of plasma are defined: thermal and non-thermal plasma [12]. The electron temperature (T_e), vibrational temperature (T_v) and rotational temperature (T_r) are used to describe the plasma's thermal properties. In thermal plasma, all three temperatures are the same because the particles inside the plasma are all in equilibrium. A non-thermal plasma has different electron, vibrational and rotational temperatures where typically the electron temperature is the highest, above 10^4 K, and the rotational temperature is the lowest [13]. When the ambient pressure is at atmospheric levels, the rotational temperature is considered equal to the temperature of the gas (T_g) around the plasma and so is taken as the macroscopic temperature of the plasma source [14, 15]. According to experimental results, the low current discharges studied in this project are typically non-thermal [15]. Thus the method for the measurement of non-thermal plasma temperature was applied to determine its temperature.

Several methods can be used to measure a plasma's temperature such as the Langmuir probe method [16], thermocouple and tungsten wire resistance measurements [17], the Boltzmann plot method [18, 19] and the 'Best-fit' method [8, 9, 20]. The Langmuir probe method is the oldest procedure of low temperature plasma diagnostics. It is based on the estimation of current and voltage characteristics, and relies on two metallic electrodes immersed into the plasma. It is intrusive to the discharge and expensive to carry out. Thermocouple and tungsten wire resistance measurement methods, also disturb the discharge channel. The measuring range of those three methods is also small, T<1500 K, and so not suitable for this project. The Boltzmann plot and 'Best-fit' methods are both based on spectroscopic diagnosis of emissions of molecules within the gas sustaining the plasma, and are more convenient than the former methods. They are non-contacted methods which do not interrupt the discharge or have influence to its electrical characteristics. A high resolution spectrometer is necessary for the Boltzmann plot method and so here the 'Best-Fit' method has been used as an economical way to measure the plasma temperature with an acceptable accuracy as it does not require a high resolution spectrometer.

The principle of the 'Best-fit' method is to compare experimental spectra with simulation results: if they fit each other well then it is considered that they have same temperature. In the fitting process the spectrometer resolution must be taken into account. The commercially available SPECAIR software [8] has been used to simulate the spectra, which is capable of modelling both thermal and non-thermal plasma.

2.2 THE N_2(C-B) MOLECULAR SYSTEM

The experiment was carried out in an open-air environment comprising O_2 (20.95%), N_2 (78.08%), Argon (0.93%) and H_2O and CO_2 molecules. During a discharge process, many molecular species are excited and photons of different wavelengths are emitted. Various spectra of those excited molecules can be observed. OH, NO(γ), O_2, N_2 (C-B) and N_2^+ (B-X) spectral systems are often used for different purposes [8, 9].

In this project, N_2(C-B) was chosen because [15]:

- N_2(C-B) is easily excitable and observed in plasma sources in environments rich in nitrogen.
- The N_2(C-B) system is well understood and it has been used as a pyrometer many times in previous research [9].
- The accuracy of the measurement is appropriate.

The typical N_2(C-B) spectrum simulated by SPECAIR is shown in Figure 1. The spectrum is sensitive to the change of plasma temperature and the peaks around 337, 357 and 380 nm are the most frequently used for temperature determination.

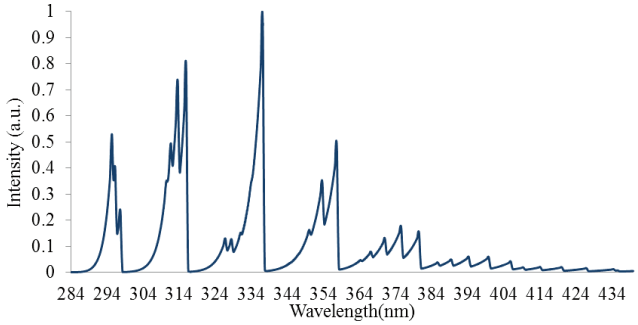

Figure 1. Simulated N_2 (2+) molecular spectrum.

2.3 EFFECT OF TEMPERATURE ON EMISSION SPECTRA

The detailed simulated spectra of the N_2 (2+) system around 337 nm, 357 nm and 380 nm with different vibrational and rotational temperature combinations are shown in Figure 2, Figure 3 and Figure 4, respectively.

In the 337 nm system, it is evident that the width of the band is sensitive to rotational temperature. It can be seen that the higher the rotational temperature, the wider the band. On the other hand, when the rotational temperature is a constant and

the vibrational temperature changes, the spectra are relatively unchanged. Accordingly, the 337 nm system can only be used to determine the rotational temperature of an arc.

In the 357 nm system of Figure 3, there are two distinct peaks, one at 357 nm and one near 353 nm. When the rotational temperature increases with a constant vibrational temperature of 4000 K, the width of the 357 nm peak increases. On the other hand, the width of the 357 nm peak is not responsive to the vibrational temperature. However, the intensity of the lower peak is sensitive to T_v, so the width of the higher peak can be used to determine the rotational temperature, and the intensity of the lower band peak can be used to measure the vibrational temperature. The intensity of the low band peak also varies with T_r. So the sequence of the measurement is to vary the model rotational temperature to fit the experimental 357 nm peak, and then change the model's vibrational temperature to fit the second peak [15]. In this way the rotational and vibrational N_2 temperatures are determined.

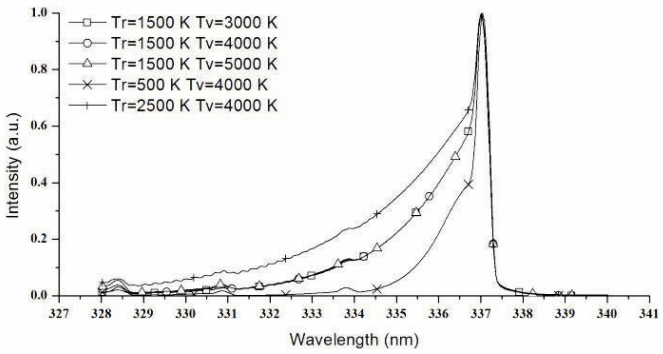

Figure 2. Simulated spectra of 337 nm system at different temperatures.

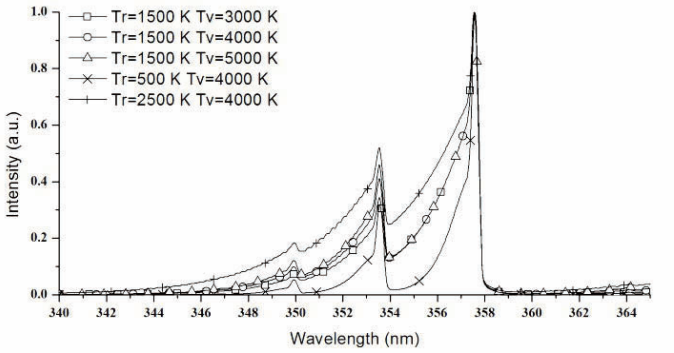

Figure 3. Simulated spectra of 357 nm system with different temperatures.

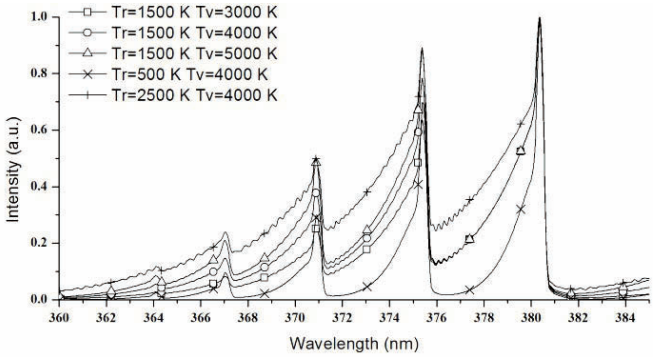

Figure 4. Simulated spectra of 380 nm system with different temperatures.

Most characteristics in the 380 nm system are similar to those in the 357 nm system. However there are more than the two distinct peaks seen at 357 nm and the emission intensity of 380 nm system is the weakest if the three systems (Figure 1).

As a result of these considerations, the 337 nm system was chosen to identify the rotational and vibrational temperatures of the discharges.

3 EXPERIMENTAL SETUP

Figure 5 shows the structure of the experiment. A 230 V, 50 Hz power source was connected to the system through a transformer with a maximum 30 kV (RMS), 30 kVA output. A ballast resistor of either 4 MΩ or 6 MΩ protected the circuit, and controlled the discharge current. An oscilloscope recorded the V-I data during the experiment: one channel was connected through a 10000:1 voltage divider, and the other was parallel to a 1 kΩ shunt resistance to measure the current.

The experiment concerns discharges between water droplets. Using metal electrodes does not provide an adequate experimental model for this situation. For example very high currents (> 0.35 amp) are needed to sustain a stable discharge between metal electrodes [21] while water sustains a stable discharge even with low current flow [22, 23]. However because of their natural dynamics in the presence of fields, generating stable droplets for such experiments is difficult [24]. A method was developed which uses a syringe with its tapered nozzle to provide a controlled a water surface. A copper wire fed into the back of the syringe gave electrical contact to the bulk water behind the syringe opening (as shown in Figure 6). This arrangement allows the discharges to be established between droplets without a solid surface between them.

Two syringes filled with tap water (σ =80 μs/cm) were introduced so that controlled water surfaces (equivalent to a 1 mL droplet) would form at their openings. A THORLABS BFH48-1000 polymer-clad optical fibre (range: 350–1200 nm) and Phantom high speed camera V7.1 were separately placed horizontally in front of the discharge path to capture the light emission and the visible images of the discharges respectively. The distance between discharge and fibre was 3 mm for the collection of overall spectra.

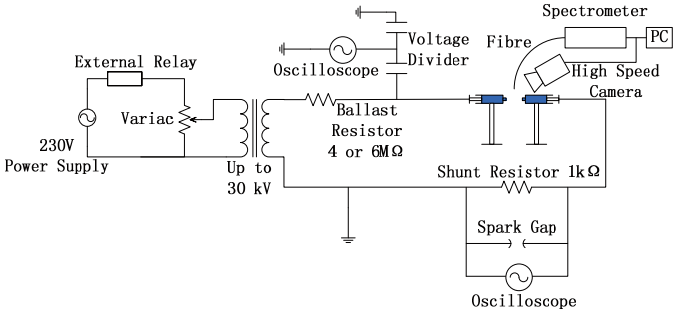

Figure 5. Experimental arrangement.

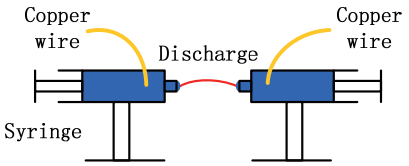

Figure 6. The use of syringes to form controlled water electrodes.

A Princeton 320PI spectrometer was utilized for processing the spectra from the optical fibre. This uses a computer optimized Czerny-Turner optical system with a 14 × 30 mm focal plane. With a 1200 g/mm grating, the resolution is up to 0.1 nm varying with the slit width. In the measurements reported here, the resolution of spectrometer is 0.313 nm. WINSPEC and SPECAIR software was used for data collection and analysis, respectively.

In the experiment described in Figure 5, the fibre receives radiation from the whole of the discharge length. Alternatively, an extra optical system could also be inserted to enable the measurement of the temperature at different points along the discharge channel. The core components of this system are two quartz lenses, illustrated in Figure 7, with a focal length of 20 cm and an optical rail for maintaining close control of the whole experiment physically. The lenses were chosen for their UV transparency, enabling the spectra around 357 nm to pass through them with minimal absorption. The first lens was placed 20 cm from the arc channel and the second just behind. The optical fibre was then also fitted on the rail at the same level of the lenses' centres to receive the focused light. The whole assembly of components could be moved horizontally along the rail, thereby collecting the light emitted from specific parts of the discharge. When setting up, a back-light was used to enhance the intensity of the image which helped to locate the optical fibre. In this way light could be analysed from spot sizes of 0.5 mm radius at any point along the discharge.

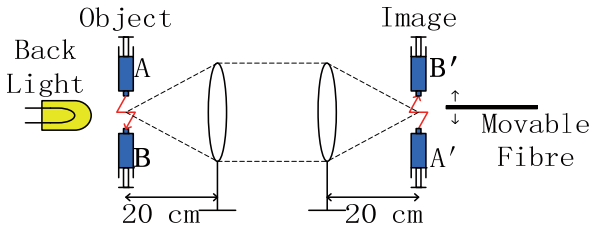

Figure 7. Optical system for probing parts along the discharge path.

Experiments determining the influence of discharges on the temperature of a silicone rubber surface were performed by putting a silicone rubber surface (3 mm) under the syringes' orifices. In this way a controlled discharge was created over the surface. In this case a Flir T400 thermal camera was implemented to measure and record the silicone surface temeprature before, during and after the discharge.

4 EXPERIMENTAL RESULTS

4.1 CURRENT AND DISCHARGE TEMPERATURE

Figure 8 shows results from discharges with no dielectric surface present for which: the gap between electrodes was set at 4 mm and the peak instantaneous current value varied from 2.5 to 5 mA in steps of 0.5 mA, by varying the voltage and using the 6 MΩ ballast resistor. The experimental arrangement was as described in Figure 5. Each step of current was held for at least 30 s, ensuring the measurements made were in equilibrium. The temperature of a discharge between water electrodes increased from 1200 K when the current was 2.5 mA, to 1500 K when the current was raised to 5 mA. A linear trend line was fitted to the data, giving a temperature:

$$T = 113I + 946 \quad (1)$$

Where T is the discharge temperature (K) and I is the discharge current (mA). The gradient is 113 K/mA with a goodness of fit, R^2, of 0.97.

4.2 RELATIONSHIP BETWEEN DURATION AND DISCHARGE TEMPERATURE

The choice of ballast resistor does not affect the point-on-wave breakdown voltage across the droplet gap. However if a higher source peak voltage is used to excite the circuit, the breakdown value is reached earlier in each half of the power frequency cycle. For the same maximum current then, the peak voltage level of the experiment with 6 MΩ resistor would increase the duration time of a discharge in each half cycle as shown in Table 1. In summary when the resistor is larger, the discharge exists for a longer period in every half cycle.

Figure 9 shows the comparison of the temperature of discharge with current. When the peak current was 3.5 mA, the durations for 4 and 6 MΩ tests were 3.73 ms and 5.52 ms respectively. With longer duration, the temperature of discharge correspondingly increased from 1200 K to 1350 K. When the maximum current level was increased to 4, 4.5 and 5 mA, the difference between the tests reduced respectively to 100, 70 and only 30 K. The energy over the discharge determined by the product of average arc resistance, the square of peak current and duration within a half cycle is plotted with plasma temperature in Figure 10. The temperature increases linearly with the elevation of discharge energy, with a gradient of 3.23 K/mJ and an R^2 of 0.87 (Equation (2)).

$$T = 3.23E + 1158 \quad (2)$$

where T is the discharge temperature (K) and E is the energy of the discharge per half cycle (mJ).

Table 1. Duration, arc resistance and energy of 4 mm discharge between water droplets for each 10 ms half power cycle.

Resistor (MΩ)	Max Current (mA)	Duration (ms)	Arc Resistance (MΩ)	Arc Energy (mJ)
4	3.5	3.73	0.67	31
	4	4.68	0.59	44
	4.5	5.45	0.56	62
	5	5.95	0.55	82
6	3.5	5.52	0.74	50
	4	6.90	0.67	74
	4.5	7.03	0.66	94
	5	7.23	0.65	117

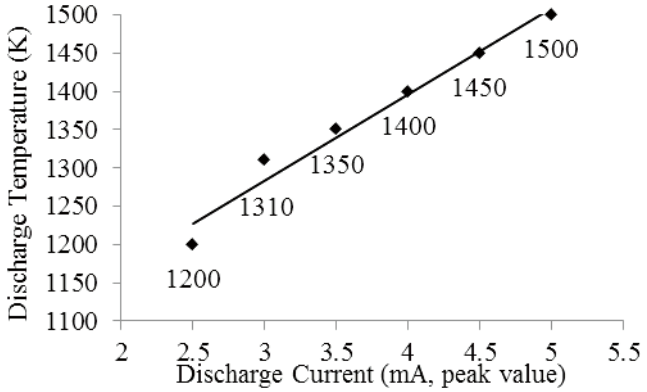

Figure 8. Temperature of 4 mm discharge (with 6 MΩ ballast resistor).

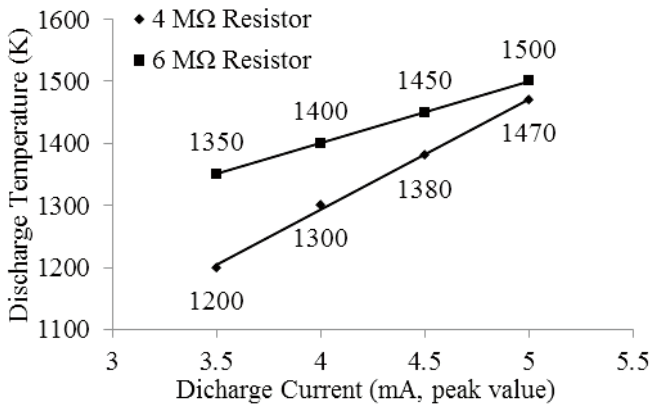

Figure 9. Temperature of discharge with different ballast resistors.

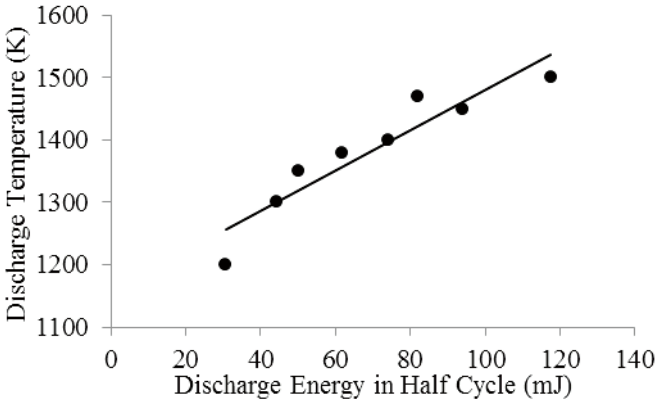

Figure 10. Relationship between discharge energy and temperature for a 4 mm discharge with different ballast resistors.

4.3 GAP LENGTH AND DISCHARGE TEMPERATURE

Four sets of experiments were carried out, using either the 4 MΩ or 6 MΩ resistor. In each the current was fixed and the discharge gap varied between 2, 4 and 6 mm. Results are shown in Figure 11. When the ballast resistor was 4 MΩ and the max current was at 4.5 mA, the discharge temperature reduced with increasing gap length. This is because as the gap length widens, the duration of the arc is diminished in each half cycle. With the current increased to 6 mA, the temperature of around 1520 K was not influenced by gap length. At lower currents with the 6 MΩ resistor, the discharge became hotter as its length increased.

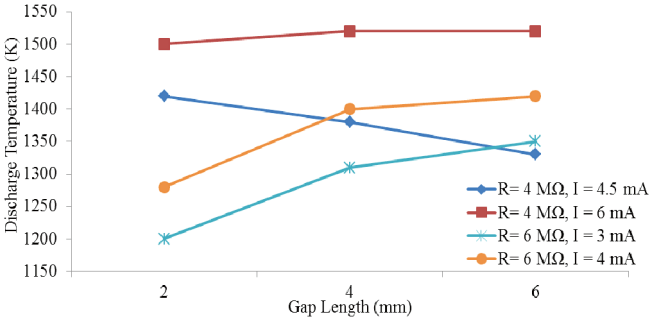

Figure 11. Temperature of discharge with different lengths.

In an attempt to understand the data in Figure 11 better, Figure 12 combines the data of Figures 10 and 11 and shows for each data point the discharge energy per half cycle plotted against discharge temperature. A linear fit yields:

$$T = 1.48E + 1239 \quad (3)$$

where T is the discharge temperature (K) and E is the energy of the discharge per half cycle (mJ). An R^2 of 0.58 shows only a weak relationship between the energy and discharge temperature. A plot of discharge energy in half cycle per unit length of discharge (mJ/mm) also indicates that no evident connection between discharge length and discharge temperature.

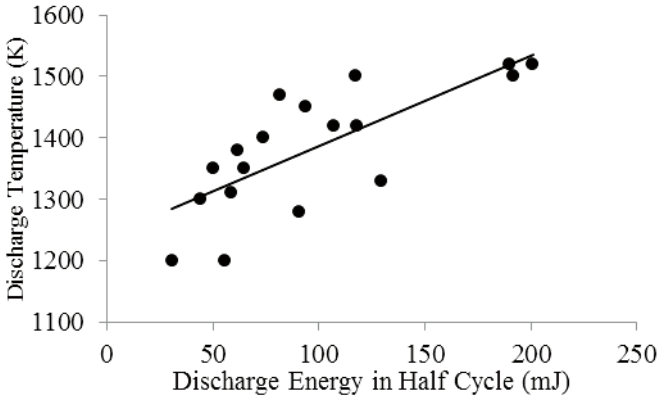

Figure 12. Relationship between discharge energy density and temperature with different discharge lengths.

4.4 TEMPERATURE ALONG DISCHARGE LENGTH

Normally, it is observed that the arc roots of an alternating current discharge are much brighter than the discharge column [24]. According to typical characteristics of plasma and discharges, for same type of plasma, the one with higher temperature emits brighter light [11], so it is generally held that the temperature changes along the length of a discharge and the arc roots have higher temperature than the arc column. The system shown in Figure 7 was implemented to determine the temperature of a discharge along its length. The gap between the water electrodes was 4 mm and considered in three parts: the area around the earthed droplet, the middle of the path and the area around the high voltage droplet. Areas of 1 mm diameter were analysed in the centre of the discharge and at the roots.

Based on the resulting data in Table 2, the hottest part of the discharge appeared at the arc column not around the roots. Occasionally, the overall temperature of the discharge was even higher than the related highest temperature among those three positions. The reason for that is considered later in this paper.

Table 2. Temperature along a 4 mm discharge.

Maximum Current (mA)	Overall Temperature (K)	Earth (K)	Mid (K)	HV (K)
2.5	1200	1100	1100	1100
3	1310	1180	1200	1100
3.5	1350	1250	1300	1120
4	1400	1300	1380	1300
4.5	1450	1350	1400	1300
5	1500	1360	1420	1310

4.5 INFLUENCE OF AN INSULATION SURFACE ON DISCHARGE TEMPERATURE

The experiments in previous sections were carried out without the presence of an insulation surface. On introduction of a silicone rubber surface, arc temperatures are seen to increase as shown in Table 3 and Figure 13. The equations of the relationships between current and temperature for the results with and without surface are shown in equation (4) and (5) respectively.

$$T = 106I+1137 \quad (4)$$

$$T = 100I + 1000 \quad (5)$$

The average elevation magnitude of arc temperature T (K) by the surface is approximately 160 K at all currents I (mA). The R^2 of equations (4) and (5) are 0.88, and 1.0 respectively. A good correlation is found between arc temperature and arc energy per half cycle in Figure 14 for discharge with and without a surface, and equation (6) results with an R^2 of 0.94.

$$T = 1.27E + 1320 \quad (6)$$

4.6 TEMPERATURE OF THE INSULATION SURFACE UNDER LOW CURRENT DISCHARGES

Figure 15 demonstrates the layout of the discharge between droplets over the SiR surface. Whilst measuring the discharge temperature over the insulation surface, the change of surface temperature was also recorded by the thermal imager. The temperature distribution over the surface, under a 4 mA discharge, between droplets separated by 4 mm reached equilibrium after being exposed to the discharge for 25 s. The thermal image of the surface at the equilibrium state is shown in Figure 16.

Table 3. Comparison of duration time, arc resistance and energy of 4 mm discharge with and without the presence of insulation surface.

Surface	Max Current (mA)	Duration (ms)	Arc Resistance (MΩ)	Arc Energy (mJ)
No	3.5	5.52	0.74	50
	4	6.90	0.67	74
	4.5	7.03	0.66	94
	5	7.23	0.65	117
Yes	3.5	7.00	1.54	132
	4	8.50	1.35	184
	4.5	9.00	1.31	239
	5	9.40	1.21	284

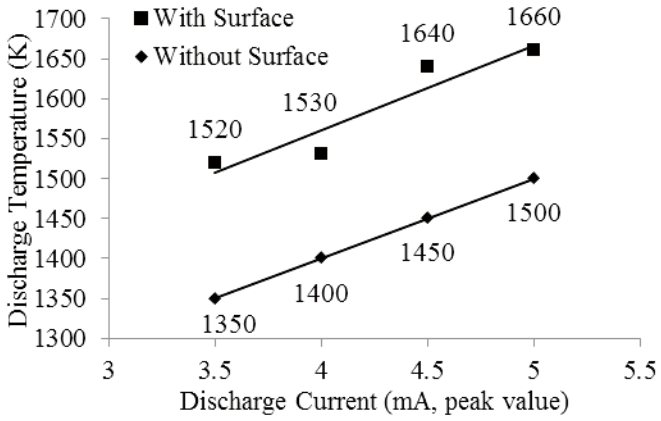

Figure 13. Comparison of discharge temperature with and without an insulating surface.

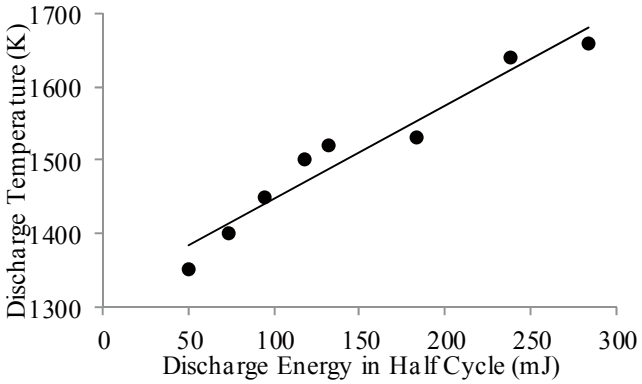

Figure 14. Relationship between discharge energy per half cycle and temperature with and without insulation surface.

Figure 16 and Figure 17 show that the surface underneath the centre of the arc column was heated the most to 305 °C and then the temperature decreased smoothly towards both electrodes to less than 150 °C. The heat distributions on the half left and right parts are quite symmetrical.

5 SIMULATION OF HEAT TRANSFER

Simulations based on finite element analysis (FEA) have been generated to build a heat transfer model to simulate the energy exchange between the discharge and the insulation surface. All the works were simulated within COMSOL.

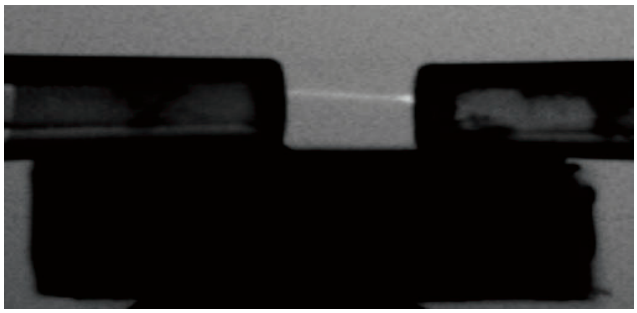

Figure 15. Discharge between droplets over insulation surface.

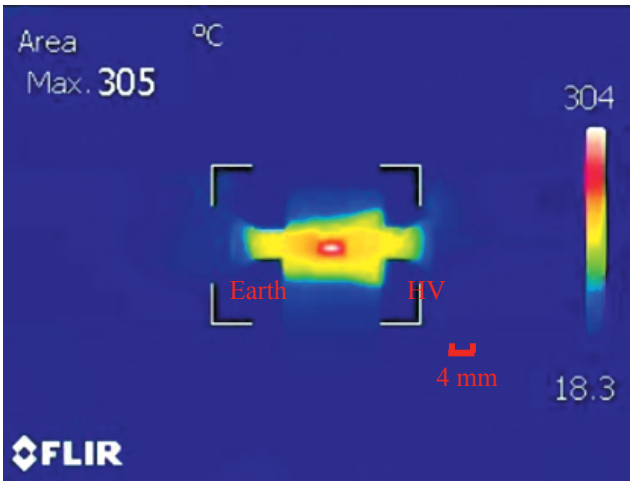

Figure 16. Thermal image of surface under discharge (Units: °C, t= 25 s).

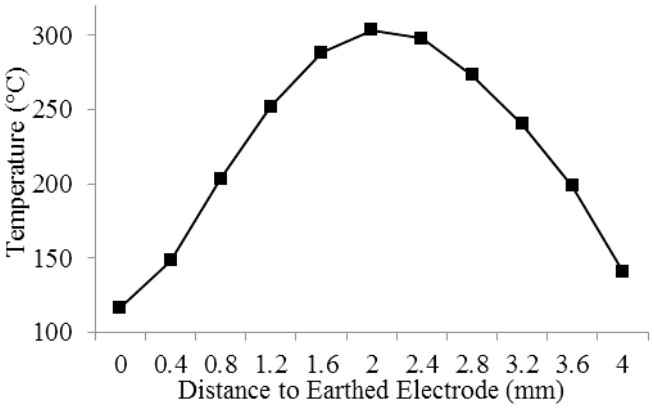

Figure 17. Experimental temperature distribution along the central line.

In practice, the heat from a discharge is transferred to its environment through conduction, convection and radiation. Kim et al [25] previously generated a model which ignored heat dissipation through radiation and convection. Comparison between various simulations with different heat transfer methods indicates that conduction dominates the heat exchange process corroborating Kim's assumption. So in the treatment described here, only the effect of conduction is considered.

Both the experimental and modelled discharges between droplets over insulation surface and the appearance of the model are shown in Figure 18. In the COMSOL model, the length of the discharge column was set at 4 mm as the temperature data used in the simulation was from the experimental results of 4 mA, 4 mm discharges. Based on the high speed video of discharge, the radius of the cross-section of the arc filament was 0.05 mm and the discharge column and roots separated 0.07 mm and 0.06 mm above the insulating surface respectively. The arc lay on two semi spherical water droplets of radius 2 mm, with contact angles of 90 degrees. A 40 mm × 20 mm × 3 mm cuboid formed the silicone rubber surface with the conductivity of 1.12 W/(mK) [26, 27]. Three segments of the arc length were initially defined and assigned temperatures of 1300 K, 1380 K, and 1300 K. The temperature used here was from experiments without the insulation surface as a first approximation. The initial plaque and air temperature is set at 20 °C (293 K). The absolute pressure was set to 1 atm.

The prediction of the model of the highest temperature on the surface is recorded in Figure 19 over the first 25 s of the arc being present. The silicone temperature rises to more than 200 °C in less than 1 second. After 5 s the temperature is around 280 °C and ultimately reaches a near-equilibrium state 20 seconds after ignition, of around 310 °C.

Figure 18. Practical and COMSOL model for heat transfer simulation

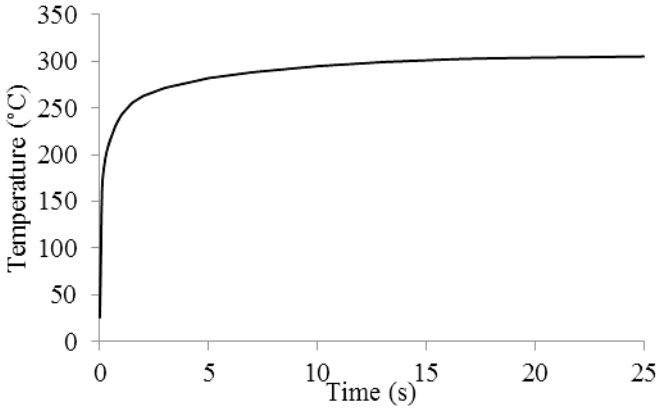

Figure 19. Maximum temperature modelled on the insulation surface.

Figure 20 shows that the model of the surface at 25 s after the ignition of the discharge. The central part of the surface has a higher temperature than the area under arc roots. The central temperature reaches 307 °C while the temperatures around the triple junctions are around 150°C. The heat distribution is symmetrical. Only 2.3 mm^2, 3% of the top surface area, and 0.4 mm^3, 0.17% of the total volume, have been heated to over 200 °C. The surface would be expected withstand this situation undamaged for an extended period of time [27].

The prediction of the temperature inside the silicone plaque is shown in Figure 21. It starts from 307 °C at the surface and then drops to 170, 125 and 100 °C at depths of 0.5, 1 and 1.5 mm respectively. The temperature at the point on the underneath surface is a little above 70°C.

Normally, a low current discharge as seen under laboratory conditions does not last as long as the simulation results shown (i.e. 25 s) [24]. Figure 22 illustrates the first second after the ignition of the discharge. The surface reaches 200 °C after 0.35 s and after 1 s the peak temperature is around 240 °C.

Simulations have been developed to show the effect of changing the thermal conductivity of the substrate to 30, 70, 130 and 170% of the original value. The change of peak temperature of the insulation surface along time is shown in Figure 23. When the thermal conductivity of the insulation has been increased by 70%, the equilibrium maximum temperature is reduced to only 190 °C. However a 70% reduction in thermal conductivity elevates the steady state temperature to over 700 °C.

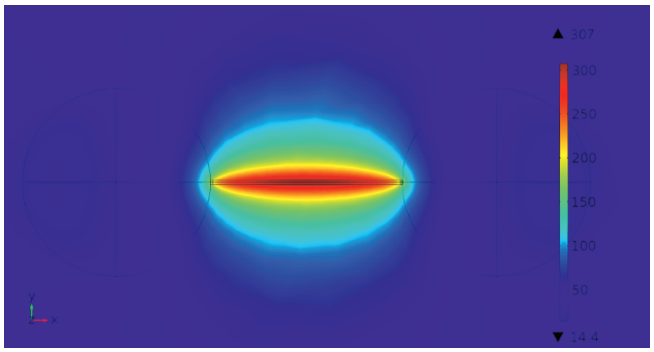

Figure 20. Temperature distribution over the insulation surface in the presence of an AC discharge (units: degree C, t= 25 s)

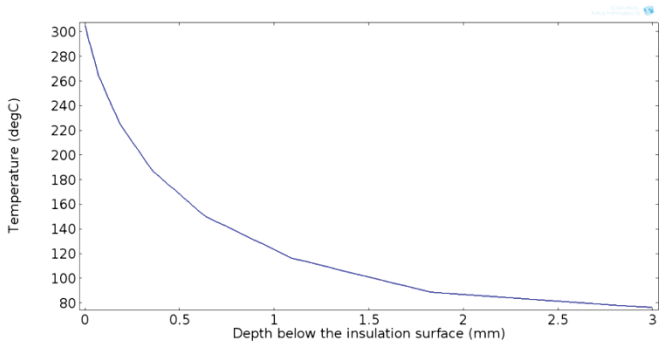

Figure 21. Maximum temperature inside the SiR plaque after 25 s.

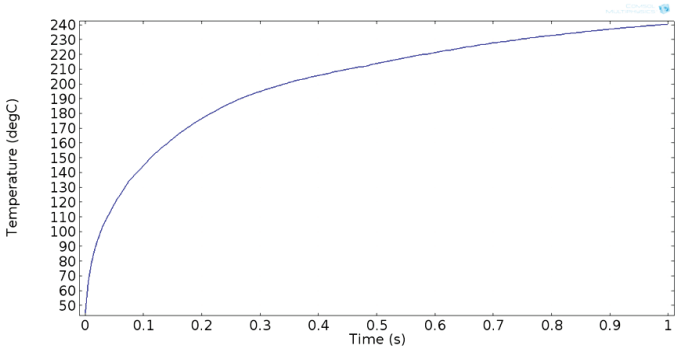

Figure 22. Growth of maximum temperature over insulation surface in the first second of a discharge being struck.

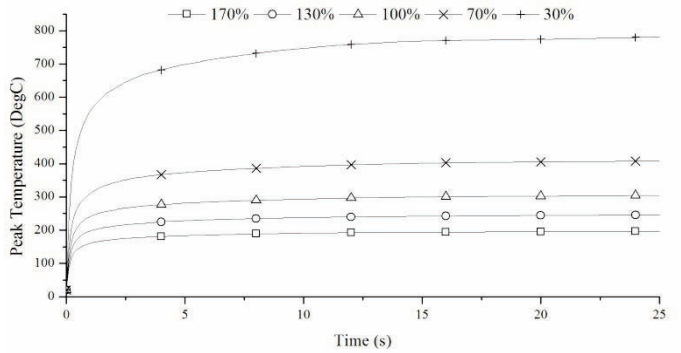

Figure 23. Maximum temperature over insulation surface with variation of thermal conductivity with time.

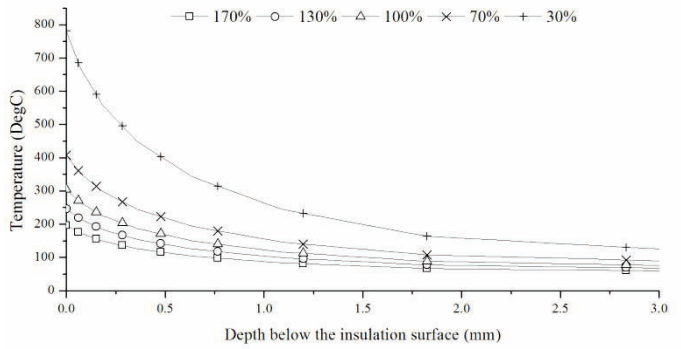

Figure 24. Equilibrium temperature inside the SiR with variation of thermal conductivity.

Figure 24 illustrates the effect of changing thermal conductivity on the temperature distribution inside the sample. When the material has very good heat dissipation ability, the temperature difference between the top surface and the bottom surface is only 120 °C. This difference gradually increases with the reduction of thermal conductivity ability and finally reaches 650 °C when the thermal conductivity goes down to 30% of the original value.

6 DISCUSSION AND CONCLUSIONS

The "Best-fit" method of optical emission spectroscopy analysis has been successfully applied to measure the discharge temperature of short, low current discharges. Experiments have been successfully carried out and the rotational nitrogen temperature varies between 1200 K and 1660 K under different conditions of current (3-5 mA) and discharge length (2-6 mm) examined. The relationship between the temperature of the low current discharge and its current has been shown to be linear, but only if the supply circuit is fixed. The temperature also increases linearly with discharge energy when the gap length is a constant, 4 mm.

Comparing discharges with different currents is complicated because the supply circuit affects the discharge duration. In particular, a higher voltage source will reach the breakdown voltage within a cycle earlier than a lower voltage source, and so provide an arc with a longer duration. Only then does the ballast resistor make a difference by controlling the source impedance and peak instantaneous current. This point can be readily modelled in the laboratory, however this does illustrate the difficulty of understanding the energy of discharges on insulators in service. In that case, the current of the discharge is controlled by the rest of the insulator surface and any other discharges in series, and the voltage before the discharge is initiated is controlled by the supply and any other high resistive features in parallel on the insulator surface. This does illustrate why insulators used on higher voltage systems see hotter discharges irrespective of local field control measures, and equivalent currents.

When the discharge temperature has been studied in three segments, the regions including the arc roots did not have a higher measured temperature than the arc column, although the roots emit visibly stronger light. There are two reasons for this. Firstly, at the arc roots the plasma is in contact with the water droplets and is able to transfer heat into that heat sink which reduces the gas temperature near that space. Secondly the arc roots are relatively stationary in space, whereas the discharge body can move a little, reducing its visible intensity. It was also observed that the measured temperature of the discharge appeared higher than the specific temperature measured at different parts. The reason for this is also because of the relative spatial movement of the discharge between droplets. When the measurement of the overall temperature is being carried out, the optical fibre is placed 3 cm away from the discharging area. The whole region in which the discharge may occur is covered by the fibre observation area (a circle with radius of 30 mm). On the other hand, only a very small area (a circle with radius of 1 mm) is being measured when the localised temperature is being measured. Occasionally, the discharge may not lie in the observation window of the fibre and the temperature of gas around that area would reduce due to the absence of heat source, the discharge.

The presence of an insulating surface increases the discharge temperature. In the experiments of discharge temperature here the discharge was up to 1 mm distant from the surface, and still had an impact: raising both discharge temperature (~160 K) and energy (on average increasing by 150%). Based on the experimental results, the phenomenon is attributed to three factors. First, the presence of insulation surface restricts the movement of water droplet electrodes which increases the duration of the discharge by a range from 1.5 ms to 2.2 ms in every half cycle as shown in Table 3. Second, the arc resistance goes up with the introduction of silicone rubber plaque by an average value of 0.7 MΩ. In the accordance of Ohm's law, with the same current and increasing in both time and resistance, the energy will increase. Third, the SiR surface obstructs the heat dissipation from the discharge.

The temperature distribution over the surface is symmetric and the centre has the highest temperature and the temperature reduces gradually towards the water droplets. This is because the water absorbs heat which cools down the local temperature. With water droplet electrodes it is normal to see erosion and degradation primarily at the central area of the surface after being exposed to the discharge for 60 s. Comparison between experiment (Figure 15) and simulation result (Figure 18) is shown in Figure 25.

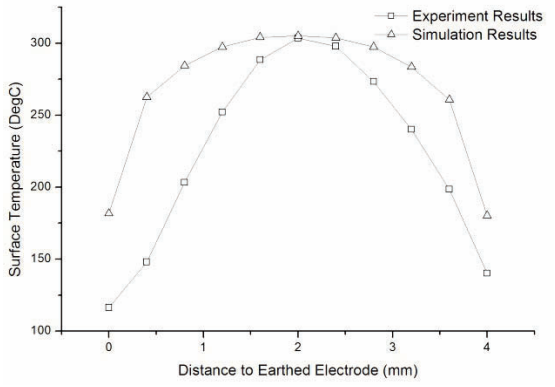

Figure 25. Comparison of temperature distribution over insulation surface between experiment and simulation result at t= 25 s.

The outcomes from the heat transfer model generally meet the observation in the experimental work. The model successfully predicts the peak temperature which dominates the ageing process. It is also shown that the central area of the surface is hotter than the surface near to the electrodes which is also observed in similar study by Xie et al [28]. In the 3 mm thick SiR sample, it was found that only very small proportion of the SiR surface would be heated to more than 200 °C. In practice, the duration of the low current discharge is normally less than a few seconds which means that the low current discharge cannot cause serious damage to the surface in such short times. The simulations with diverse thermal conductivities show that an increase of thermal conductivity reduces the surface temperature, but increasing the thermal conductive presents a threat to the surface under these conditions.

7 CONCLUSIONS

Optical emission spectroscopy analysis has been successfully applied to measure the discharge temperature of short, low current discharges between water droplets. The temperature of AC discharges had been shown to be linearly dependent on the current over the range 3-5 mA with a fixed supply circuit. However it has been shown that the temperature is dependent on the supply voltage and supply impedance as a result of the importance of the duration of a discharge in each half-cycle. The presence of an insulating surface increases the discharge temperature: raising both discharge temperature (~160 K) and its energy per half cycle (increasing by 150%).

An FEA model of heat transfer has successfully been developed and has shown the importance of the substrate thermal conductivity on its maximum surface temperature, and that the thermal conductivity of the water droplets themselves plays a role in surface temperature moderation.

ACKNOWLEDGMENT

The authors are grateful to National Grid (UK) and EPSRC (EP/G01244X/1) for the support which enabled this work. Underlying research data can be obtained from s.rowland@manchester.ac.uk.

REFERENCES

[1] R. Gorur, E. Cherney, and J. Burnham, *Outdoor Insulators,* Phoenix, Ariz., USA, 1999.

[2] K. Papailiou and F. Schmuck, *Silicone Composite Insulators: Materials, Design, Applications*, Springer, 2013, p. 250.

[3] F. B. Hampton, "Flashover mechanism of polluted insulation," Proc. IEE, pp. 985–990, 1964.

[4] A. Pillai and R. Hackam, "Effects of glow discharge conditioning and addition of gases on surface flashover," IEEE Trans. Electr. Insul., Vol. 20, No. 4, pp. 763–767, 1985.

[5] X. Zhang and S. Rowland, "Modelling of dry-band discharge events on insulation surfaces," IEEE Int'l. Sympos. Electr. Insul. (ISEI), pp. 1–5, 2010.

[6] X. Zhang and S. M. Rowland, "Stability and energy of low current surface discharges on wet surfaces," IEEE Trans. Dielectr. Electr. Insul., Vol. 19, No. 6, pp. 2055–2062, 2012.

[7] S. Rowland, K. Kosidas, and X. Zhang, "Aging of polyethylene ADSS sheath by low currents," IEEE Trans. Power Deliv., Vol. 25, No. 2, pp. 947–952, 2010.

[8] C. O. Laux, T. G. Spence, C. H. Kruger, and R. N. Zare, "Optical diagnostics of atmospheric pressure air plasmas," Mech. Eng., Vol. 125, 2003.

[9] D. Staack, B. Farouk, A. F. Gutsol, and A. A. Fridman, "Spectroscopic studies and rotational and vibrational temperature measurements of atmospheric pressure normal glow plasma discharges in air," Plasma Sources Sci. Technol., Vol. 15, No. 4, pp. 818–827, 2006.

[10] D. Staack, B. Farouk, A. Gutsol, and A. Fridman, "Characterization of a dc atmospheric pressure normal glow discharge," Plasma Sources Sci. Technol., Vol. 14, No. 4, pp. 700–711, 2005.

[11] S. Haydon and L. Talbot, *An Introduction to Discharge and Plasma Physics,* The University oof New England and Queensland, 1965.

[12] M. I. Boulos, P. Fauchais, and E. Pfender, *Thermal Plasmas: Fundamentals and Applications*, Vol. 1. New York; London: Plenum Press, p. 452, 1994.

[13] C. Laux, R. Gessman, and C. Kruger, "Rotational temperature measurements in air and nitrogen plasmas using the first

negative system of N 2+," J. Quant. Spectrosc. Radiat. Transf., Vol. 68, No. 4, pp. 473–482, 2001.

[14] O. Motret and C. Hibert, "Rotational temperature measurements in atmospheric pulsed dielectric barrier discharge-gas temperature and molecular fraction effects," J. Phys. D. Appl. Phys., Vol. 33, No. 12, pp. 1493–1498, 2000.

[15] A. Xiao, S. M. Rowland, J. C. Whitehead, and X. Tu, "Temperature measurement of low-current discharges based on N 2 (2 +) molecular emission spectra," IEEE Conf. Electr. Insul. Dielectr. Phenomena (CEIDP), Vol. 2, pp. 191–194, 2012.

[16] R. Hippler, S. Pfau, M. Schmidt, and K. H. Schoenbach, *Low Temperature Plasma Physics: Fundamental Aspects and Applications,* Weinheim; Cambridge: Wiley-VCH, 2001, p. 590.

[17] S. Pellerin, J. M. Cormier, F. Richard, K. Musiol, and J. Chapelle, "A spectroscopic diagnostic method using UV OH band spectrum," J. Phys. D (Applied Physics), vol. 29, no. 3, pp. 726–39, 1996.

[18] C. De Izarra, "UV OH spectrum used as a molecular pyrometer," J. Phys. D. Appl. Phys., Vol. 33, No. 14, pp. 1697–1704, 2000.

[19] X. Tu, B. G. Chéron, J. H. Yan, and K. F. Cen, "Electrical and spectroscopic diagnostic of an atmospheric double arc argon plasma jet," Plasma Sources Sci. Technol., Vol. 16, No. 4, pp. 803–812, 2007.

[20] X. Tu, H. J. Gallon, and J. C. Whitehead, "Electrical and spectroscopic diagnostics of a single-stage plasma-catalysis system: effect of packing with TiO 2," J. Phys. D. Appl. Phys., Vol. 44, No. 48, p. 482003, 2011.

[21] J. D. Cobine and G. a. Farrall, "Experimental Study of Arc Stability. I," J. Appl. Phys., Vol. 31, No. 12, p. 2296-2304, 1960.

[22] P. Bruggeman and C. Leys, "Non-thermal plasmas in and in contact with liquids," J. Phys. D. Appl. Phys., Vol. 42, No. 5, p. 053001, 2009.

[23] P. Bruggeman and J. Liu, "DC excited glow discharges in atmospheric pressure air in pin-to-water electrode systems," J. Phys. D. Appl. Phys., Vol. 41, No. 21, p. 215201, 2008.

[24] S. M. Rowland and F. C. Lin, "Stability of alternating current discharges between water drops on insulation surfaces," J. Phys. D. Appl. Phys., Vol. 39, No. 14, pp. 3067–3076, 2006.

[25] S. H. Kim and R. Hackam, "Temperature distribution in RTV silicone rubber coating following dry band arcing," IEEE Int'l. Sympos. Electr. Insul., Pittsburgh, PA USA, pp. 599–602, 1994.

[26] Q. Wang, W. Gao, and Z. Xie, "Highly thermally conductive room temperature vulcanized silicone rubber and silicone grease," J. Appl. Polym. Sci., pp. 4–6, 2003.

[27] S.-E. Silicone, "Characteristic properties of Silicone Rubber Compounds," *Silicone, Shin-Etsu*, 2012. [Online]. Available: http://www.silicone.jp/e/catalog/pdf/rubber_e.pdf. [Accessed: 28-Jan-2014].

[28] G. Xie, J. Luo, Y. Yang, D. Guo, and L. Si, "Water droplets on a hydrophobic insulator surface under high voltages: A thermal perspective," Appl. Phys. Lett., Vol. 101, No. 13, 131602, 2012.

An Xiao was born in Jiangxi province, China. He completed the B.Eng. degree in Nanjing University of Posts & Telecommunication. He received the MSc. Degree with distinction in electrical power systems from the University of Manchester in 2010, where he is currently doing his Ph.D. degree study. His main research interests include spectroscopic diagnostics of different discharge, heat transfer between discharge and insulation surface and the ageing of outdoor insulators.

Simon M. Rowland (SM '07-F '14) was born in London, England. He completed the B.Sc. degree in physics at The University of East Anglia and the Ph.D. degree at London University. He was awarded the IEE Duddell Premium in 1994 and became a FIEE in 2000. He has worked for many years on dielectrics and their applications and has also been Operations and Technical Director within multinational manufacturing companies. He joined The School of Electrical and Electronic Engineering in The University of Manchester as a Senior Lecturer in 2003, and was appointed Professor of Electrical Materials in 2009. He served as President of the IEEE Dielectric and Electrical Insulation Society during 2011–2012.

Xin Tu (M'12) was born in Zhejiang Province, China. He completed the Ph.D. degree in Physics at CORIA, University of Rouen (France) and the Ph.D. degree in Thermal Power Engineering at Zhejiang University (China). He was a Postdoctoral Fellow with the Center for Surface Chemistry and Catalysis, Katholieke Universiteit Leuven, Leuven, Belgium, and then moved to The University of Manchester, working as a Research Associate in the School of Chemistry. He joined the Department of Electrical Engineering and Electronics at the University of Liverpool as a Lecturer in 2012. He has worked for many years on interdisciplinary research at the interface of plasma physics and plasma chemistry directed towards energy conversion and environmental pollution control.

Christopher Whitehead was born in Edinburgh, Scotland and educated at the Universities of Edinburgh (B.Sc. in chemical physics) and Cambridge (Ph.D.). After holding a Royal Commission for the Exhibition of 1851 Fellowship at Cambridge and a Lindemann Trust Fellowship at Columbia, New York, he joined the University of Manchester in 1977. As a physical chemist, his research interests lie in the area of the chemistry and spectroscopy of excited states which have included the topics of combustion, chemical lasers and, most recently, atmospheric pressure plasma. He was appointed Professor of Chemistry in 2004 and is presently Head of the School of Chemistry at Manchester.